Spin-dynamics study of the classical ferromagnetic XY chain in a random field

R. W. Gerling*
HLRZ, c/o Forschungszentrum Jülich G.m.b.H. (KFA) 5170 Jülich, Germany

D. P. Landau
Center for Simulational Physics, University of Georgia, Athens, Georgia 30602
(Received 8 September 1992)

The classical one-dimensional XY model in a symmetry-breaking Gaussian-distributed random magnetic field was studied using an ultrafast, vectorized spin-dynamics program on a Cray Y-MP. We calculated the time and space-displaced spin-spin correlation functions, which was then Fourier-transformed to get the neutron-scattering law $S(q,\omega)$. We see a clear change of the different contributions when the random field is switched on. At low temperatures the random field induces significant increases in the soliton density.

I. INTRODUCTION

The behavior of (pseudo-)one-dimensional systems has proven to be rich and varied, and there is extensive literature detailing studies of different aspects of this behavior. In particular, there has been great interest in the study of magnetic chains subject to symmetry-breaking fields for several reasons. This was due in part because of the beautiful experimental results[1-7] for quasi-one-dimensional systems and in part due to detailed theoretical predictions[8-10] obtained by mapping an easy-plane spin chain onto the sine-Gordon model. Particular emphasis was placed on understanding the inelastic neutron-scattering data which showed spin-wave and two-spin-wave excitations as well as central peaks which had soliton and/or two-spin-wave origins. This work prompted detailed computer-simulation studies of simple models of soliton-bearing magnetic chains.[11-18] Questions have also been raised about the effects of other interactions of linear-chain behavior.[19] For example, Endoh *et al.*[20] have examined spin fluctuations in a random chainlike magnetic system and de Groot *et al.*[21] have looked at the behavior of a magnetic-chain compound with alternating exchange. Theoretical work by José[22] probed static and dynamic properties of a random exchange Heisenberg chain model. We wish to study the effect of randomness on soliton behavior in magnetic chains. In order to compare directly with the corresponding properties of a pure system, we simulated the xy chain in a random magnetic field distributed about some nonzero value; as the field distribution becomes narrow, the model approaches the XY chain in a uniform field for which we have extensive data. The Hamiltonian of the XY chain in a random magnetic field is given by

$$\mathcal{H}_{xy}=-J\sum_{i=1}^{N}(S_i^xS_{i+1}^x+S_i^yS_{i+1}^y)-\sum_{i=1}^{N}h_iS_i^x\ , \tag{1}$$

where the $\mathbf{S}_i$ are three-dimensional classical vectors of unit length and J is the exchange-coupling constant. The exchange anisotropy makes it energetically favorable for the spins to lie in the xy plane. $h_i=g\mu_BH_i$ is an external magnetic field in the x direction; the magnetic field at each site is frozen and is characterized by a Gaussian distribution function

$$p(h_i)=\frac{1}{(2\pi\sigma^2)^{1/2}}\exp\left[-\frac{(h_i-\bar{h})^2}{2\sigma^2}\right]\ , \tag{2}$$

where $\bar{h}$ is the average magnetic field and the variance σ^2 gives the width of the distribution.

In Sec. II of this paper, we briefly describe the simulational method used, and in Sec. III we present the results of our simulations.

II. METHOD

A standard importance-sampling Monte Carlo[23] technique was used to generate equilibrium spin configurations for a given chain length of $N=20\,000$ sites with a periodic boundary. Spin updates were performed using a two-sublattice decomposition and a vectorized algorithm on a Cray Y-MP8/832. The first 3000 Monte Carlo steps (MCS)/site were always discarded to ensure that the system had reached equilibrium, and then ten spin configurations, each separated by 200 MCS/site, were chosen as starting configurations for the spin-dynamics calculation. (The separation by 200 MCS/site ensured that the configurations were uncorrelated.)

The random field h_i was calculated from Gaussian-distributed random numbers η_i with zero mean and unit variance by the transformation

$$h_i=\sigma\eta_i+\bar{h}\ , \tag{3}$$

where $\bar{h}$ is the mean value of the field and σ is the width of the field distribution. The Gaussian-distributed random numbers η_i were produced with the Box-Muller[24] method. This method uses two random numbers x_1 and x_2 from a uniform distribution in the interval [0,1] to produce two Gaussian-distributed random numbers η_i and η_2:

$$\eta_1=(-2\ln x_1)^{1/2}\cos(2\pi x_2)\ ,$$
$$\eta_2=(-2\ln x_1)^{1/2}\sin(2\pi x_2)\ . \tag{4}$$

The random numbers η_1 and η_2 are independent and have unit variance. This method is exact and fast (because it uses fewer calls to the random-number generator) as compared with the common method of summing up 12 random numbers.[25] Figure 1 shows a comparison of the theoretical distribution function $p(h_i)$ with the measured distribution for $\sigma=0.10$. The figure also shows the theoretical distribution functions for the different values of σ we used. Note that, starting with $\sigma=0.15$, a substantial percentage of the lattice sites experiences a magnetic field parallel to the negative x axis. We used different seeds for the random-number generator RANF for the part of the program which generated the random-field configuration and for the Monte Carlo part, so that we could vary the sequence of random numbers in both parts of the program independently. Data were generated for two different realizations of the random field and four different sequences of random numbers for the Monte Carlo part, so that all results represent averages over eight different runs. This totals 80 different starting configurations for the time integration.

The equation of motion for each spin in the xy model is[16]

$$\dot{\mathbf{S}}_i=\mathbf{S}_i\times[J(S_{i+1}^x+S_{i-1}^x)\mathbf{e}_x+J(S_{i+1}^y+S_{i-1}^y)\mathbf{e}_y+h_i\mathbf{e}_x]\ , \tag{5}$$

where $\mathbf{e}_x$ and $\mathbf{e}_y$ are unit vectors in the x and y directions. The coupled nonlinear equations of motion were integrated using a vectorized, high-speed fourth-order predictor-corrector method and a time-integration interval $\Delta=0.01/J$. Since the algorithm is not self-starting, the first few time steps were integrated using a fourth-order Runge-Kutta method. Each initial configuration was integrated out to time $t_{\max}=100/J$.

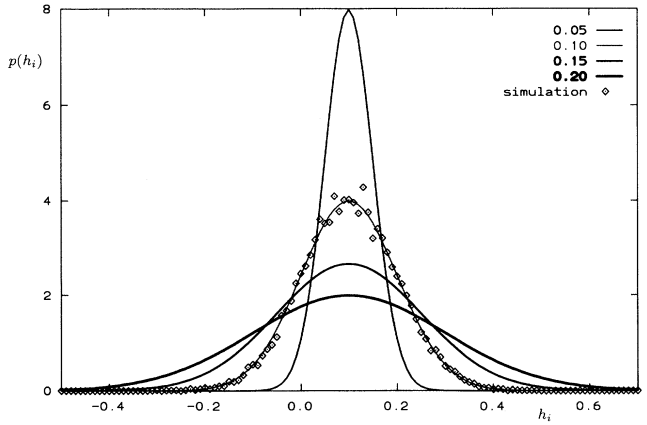

FIG. 1. Theoretical probability distribution $p(h_i)$ as a function of h_i for different values of σ as indicated and the mean value $\bar{h}=0.1J$. The area under the curves is normalized to unity. The data points represent a histogram from a realization of the random field with $N=20\,000$ spins and $\sigma=0.10$.

From the results of the time integration for each starting configuration, we calculated the time- and space-dependent spin-spin correlation functions. The correlation functions were averaged over the ten starting configurations for each run and then used as input for the last step of the program, which performed a double Fourier transform to yield the scattering law $S_k(q,\omega)$. To reduce cutoff effects, we introduced a Gaussian spatial and temporal resolution function

$$\exp\{-\tfrac{1}{2}[(r\delta r)^2+(t\delta t)^2]\}\ . \tag{6}$$

The spatial cutoff parameter was set to $\delta r=0.015$, and the temporal cutoff parameter was chosen $\delta t=0.02J$. (More details of the algorithm and testing can be found in Ref. 18.)

The fact that we have to use a resolution function produces a very close correspondence between our results and real experimental neutron-scattering data, where the resolution function of the spectrometer has to be taken into account.[26]

III. RESULTS

We concentrated our simulations on two different temperatures $k_BT=0.2J$ and $0.3J$. The first temperature ensures a sufficiently high density of spin waves, so that two-spin-wave processes are clearly visible, while the soliton density for the uniform-field model can be neglected. The second, higher-temperature allows an identification of a soliton contribution in addition to the two-spin-wave contributions, but it is still low enough to avoid the broadening of all structures which occurs at higher temperatures. For higher temperatures the identification of the different structures becomes more and more difficult.

The first question which we wished to answer was how the random field influences the soliton density. We expect the number of solitons to increase as a result of the random field, and because there is no standard operator whose thermal average gives the soliton density, the only way to determine the soliton density is to count the solitons. In Fig. 2 we show a plot of the phase of the spins in the xy plane. A soliton can be identified by a jump of the phase of $\pm2\pi$, and in this plot four solitons can be identified. In Fig. 2 single spins cannot be identified, but in an enlargement the phases of individual spins are visible, showing that a soliton is a smooth jump in phase. The difference in phase angle between nearest-neighbor spins, however, is small compared to 2π. The soliton density was determined automatically from plots such as Fig. 2. In Fig. 3 we show how the soliton density increases with increasing width of the random-field distribution. For the lowest temperature, the soliton density increases by a factor of 10 over the range of distribution widths which we studied. For the highest temperature $k_BT=0.4J$, no increase can be observed, but this is probably an artifact of our method for measuring the soliton density. If the fluctuations due to spin waves become too large, our method of detecting solitons no longer works; it is then impossible to tell the difference between a large spin-wave fluctuation and two solitons which are close to each other. Solitons can only be identified properly if the

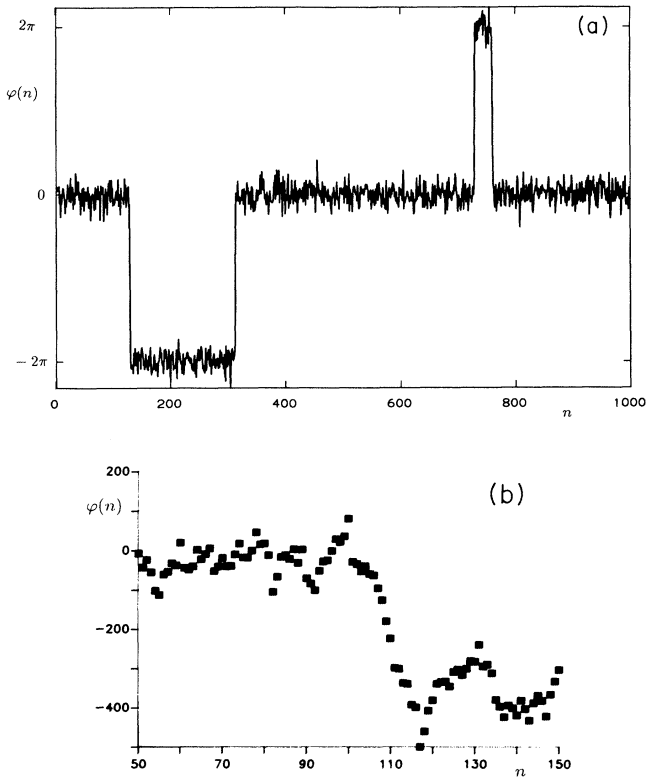

FIG. 2. In-plane phase of the spins along the chain. $k_BT=0.3J$ and $\sigma=0.05J$. Four solitons can be seen.

typical fluctuations due to spin waves are less than about $2\pi/3$.

The neutron-scattering law with polarization along the chain axis $S_z(q,\omega)$ is expected to show single spin-wave excitations, and indeed the results of the simulation show a clear single peak for each q value. Figure 4 shows our results for $S_z(q,\omega)$ for $k_TT=0.2J$ and $qa=\pi/8$ as a function of ω. With increasing width σ, the peaks broaden and shift to a slightly lower position, thus indicating a softening of the dispersion relation. In addition,

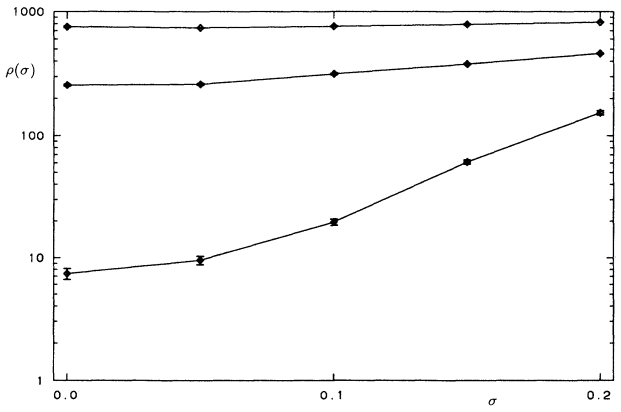

FIG. 3. Soliton density as a function of the width σ of the random field. The temperatures from bottom to top are $0.2J/k_B$, $0.3J/k_B$, and $0.4J/k_B$.

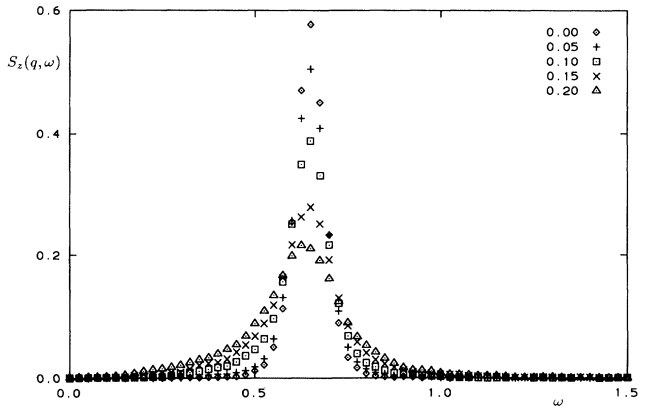

FIG. 4. Neutron-scattering law $S_z(q,\omega)$ as a function of ω. The temperature $k_BT=0.2J$, the mean value of the field $\bar{h}=0.1J$, and the wave vector $qa=\pi/8$. The value of σ is as indicated.

with increasing width of the random-field distribution, the peak becomes slightly asymmetric. The same type of asymmetry has also been observed for the anisotropic Heisenberg model.[27] (The data for the anisotropic Heisenberg model suggest that this structure is actually a separate multi-spin-wave contribution in the left shoulder of the spin-wave peak whose intensity scales with the intensity of the spin-wave peak.)

From the positions of the spin-wave peaks in the z and y polarizations, we determine the dispersion relations, which are shown in Fig. 5 for $k_BT=0.2J$ and $0.4J$. A softening of the dispersion with increasing temperature can be observed. The thick line is the dispersion for the sine-Gordon model, and medium line is the result for the harmonic approximation, which is

$$\omega(q)=\sqrt{(2+h)[2+h-2\cos(qa)]} \tag{7}$$

for the xy model. This form of the dispersion relation

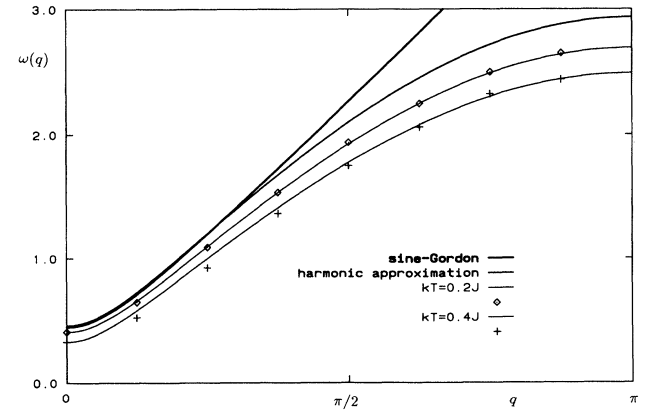

FIG. 5. Dispersion relation $\omega(q)$. The thick line is the result for the sine-Gordon theory, and the medium line is the result for the harmonic approximation from Eq. (7). The thin lines are fits to the data with a parametrized version of Eq. (7). The magnetic field is $\bar{h}=0.1J$ and the width $\sigma=0$.

was used to fit the finite-temperature result; it was parametrized as

$$\omega(q)=\sqrt{a-b\cos(q)}\ , \tag{8}$$

where a and b were fitting variables. The fits to Eq. (8) are shown by the thin lines.

For the polarization perpendicular to both the chain axis and magnetic field, $S_y(q,\omega)$, a Gaussian central soliton peak is expected[9] in addition to the spin-wave peak. Figure 6 shows our results for $S_y(q,\omega)$ for five different values of σ. The spin-wave peak shifts with increasing width σ to a slightly lower position and broadens. The new structure, which we already saw in the z polarization, is much more pronounced here. The central soliton peak, which on this scale is almost invisible for zero width of the random field, increases in intensity in proportion to the soliton density.

For the polarization along the magnetic field, we expect[9] three contributions to the neutron-scattering law $S_x(q,\omega)$: a central Gaussian soliton peak, an almost steplike line shape for the two-spin-wave difference process, and a square-root singularity at $2\omega(q/2)$ for the two-spin-wave sum process. In Fig. 7 we can see that our data for $k_BT=0.3J$ and $h=0.1J$ can be explained in terms of these three contributions. Note that the solid line is not a fit to the data points, but is the theoretical prediction. The position of the two-spin-wave sum peak was determined from the fitted dispersion relation in Fig. 5 by the expression $2\omega(q/2)$. The soliton contribution was obtained via a fit of the soliton contribution in the y polarization, which was then transformed by using the relation

$$S^x_{\rm sol}(q,\omega)=\tanh\frac{\pi q}{2m}S^y_{\rm sol}(q,\omega) \tag{9}$$

from Ref. 9. The effective mass parameter $m=\sqrt{h/J}$.

Figure 8 shows our results for $S_x(q,\omega)$ for five different values of the width σ. The temperature is $k_BT=0.3J$. The two-spin-wave difference process is substantially broadened and shifted to a lower frequency: In comparison with the shift of the single-spin-wave peak, from Fig. 4, we find that the shift is about twice as much. This also shows that the peak position of the two-spin-wave sum process is given by $2\omega(q/2)$. Under the assumption that the shift in position is independent of q, which is almost true for small values of q, the two-spin-wave sum peak is shifted twice as much as the single-spin-wave peak. The intensity of the central soliton peak increases very strongly with increasing width of the field distribution as in the y polarization.

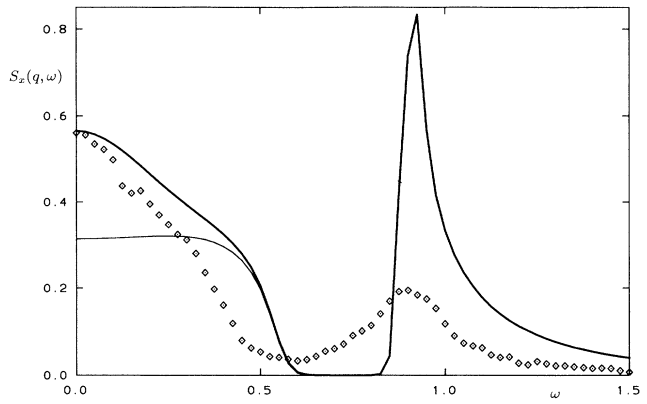

FIG. 7. Neutron-scattering law $S_x(q,\omega)$ as a function of ω. The temperature $k_BT=0.3J$, the wave vector $qa=\pi/8$, and the mean value of the field $\bar{h}=0.1J$. The width of the field distribution is $\sigma=0$. The solid curve is the theoretical prediction of Ref. 9 convoluted with our resolution function. The thin line separates the central peak in a soliton part (Gaussian peak, top part) and the two-spin-wave difference process (steplike line shape, bottom part).

IV. CONCLUSIONS

Using spin-dynamics simulations, we have calculated $S(q,\omega)$ for XY chains in a random magnetic field along the x axis. We find that the elementary excitations survive for some moderate width of the distribution function for the magnetic field. In the x and y polarizations (in

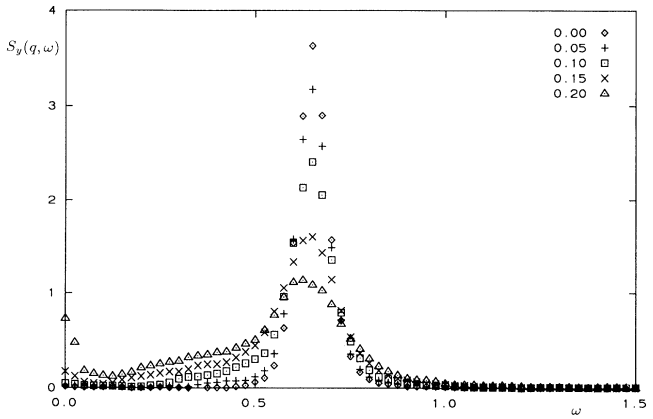

FIG. 6. Neutron-scattering law $S_y(q,\omega)$ as a function of ω. The temperature $k_BT=0.2J$, the wave vector $qa=\pi/8$, and the mean value of the field $\bar{h}=0.1J$. The value of σ is as indicated.

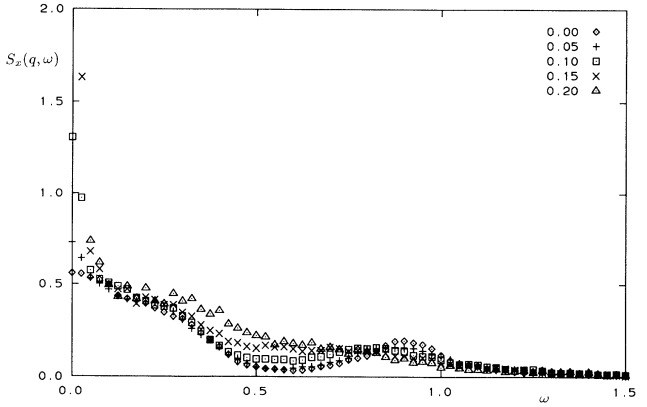

FIG. 8. Neutron-scattering law $S_x(q,\omega)$ as a function of ω. The temperature $k_BT=0.3J$, the wave vector $qa=\pi/8$, and the mean value of the field $\bar{h}=0.1J$. The value of σ is as indicated.

plane), very sharp central peaks develop with increasing width of the distribution. The polarization along the chain axis (out of plane) shows the least change with increasing width.

ACKNOWLEDGMENT

This work was supported in part by NSF Grant No. DMR-9100692.

*Permanent address: Institut für Theoretische Physik I der Universität Erlangen-Nürnberg, Staudtstrasse 7, W-8520 Erlangen, Germany.

[1]M. Steiner, J. Villain, and C. G. Windsor, Adv. Phys. **25**, 87 (1976).

[2]M. Steiner, K. Kakurai, and J. K. Kjems, Z. Phys. B **53**, 117 (1983).

[3]A. P. Ramirez and W. P. Wolf, Phys. Rev. Lett. **49**, 227 (1982).

[4]J. P. Boucher, L. P. Regnault, J. Rossat-Mignot, J. P. Renard, J. Bouillot, and W. G. Stirling, J. Appl. Phys. **52**, 1956 (1982); J. P. Boucher, L. P. Regnault, A. Pires, J. Rossat-Mignot, Y. Henry, J. Bouillot, W. G. Stirling, and J. P. Renard, in *Magnetic Excitations and Fluctuations,* edited by S. W. Lovesey, U. Balucani, F. Borsa, and V. Tognetti (Springer, Berlin, 1984).

[5]F. Borsa, Phys. Rev. B **25**, 3430 (1982); F. Borsa, M. G. Pini, A. Rettori, and V. Tognetti, *ibid.* **28**, 5173 (1983).

[6]K. Kopinga, A. M. C. Tinus, and W. J. M. de Jonge, Phys. Rev. B **29**, 2868 (1984): A. M. C. Tinus, W. J. M. de Jonge, and K. Kopinga, *ibid.* **32**, 3154 (1985).

[7]T. Goto and Y. Yamaguchi, J. Phys. Soc. Jpn. **50**, 2133 (1981).

[8]H. J. Mikeska, J. Phys. C **11**, L29 (1978).

[9]E. Allroth and H. J. Mikeska, Z. Phys. B **43**, 209 (1981).

[10]C. Etrich, H. J. Mikeska, E. Magyari, H. Thomas, and R. Weber, Z. Phys. B **62**, 97 (1985).

[11]R. W. Gerling and D. P. Landau, J. Magn. Magn. Mater. **45**, 267 (1984).

[12]R. W. Gerling and D. P. Landau, in *Magnetic Excitations and Fluctuations,* edited by S. W. Lovesey, U. Balucani, F. Borsa, and V. Tognetti (Springer, Berlin, 1984).

[13]M. Staudinger, R. W. Gerling, C. S. S. Murty, and D. P. Landau, J. Appl. Phys. **57**, 3335 (1985).

[14]R. W. Gerling, M. Staudinger, and D. P. Landau, J. Magn. Magn. Mater. **54-57**, 819 (1986).

[15]D. P. Landau, R. W. Gerling, and M. S. S. Challa, in *Magnetic Excitations and Fluctuations II,* edited by U. Balucani, S. W. Lovesey, M. G. Rasetti, and V. Tognetti (Springer, Berlin, 1987).

[16]R. W. Gerling and D. P. Landau, Phys. Rev. B **37**, 6092 (1988).

[17]R. W. Gerling, Comput. Phys. Rep. **7**, 93 (1988).

[18]R. W. Gerling and D. P. Landau, Phys. Rev. B **41**, 7139 (1990).

[19]L. J. de Jongh, J. Appl. Phys. **53**, 8018 (1982).

[20]Y. Endoh, G. Shirane, R. J. Birgeneau, and Y. Ajiro, Phys. Rev. **19**, 1476 (1979).

[21]H. J. M. de Groot, L. J. de Jongh, R. D. Willett, and J. Reedijk, J. Appl. Phys. **53**, 8038 (1982).

[22]J. V. José, in *Magnetic Properties of Low-Dimensional Systems,* edited by L. M. Falicov and J. L. Moron-Lopez (Springer, Heidelberg, 1986).

[23]K. Binder and D. P. Landau, Phys. Rev. B **13**, 1140 (1976).

[24]G. E. P. Box and M. M. Muller, Ann. Math. Stat. **29**, 610 (1958).

[25]*Handbook of Mathematical Functions,* edited by M. Abramowitz and I. R. Stegun (Dover, New York, 1964).

[26]R. J. Birgeneau, J. Skalyo, and G. Shirane, Phys. Rev. B **3**, 1736 (1971); I. U. Heilmann, G. Shirane, Y. Endoh, R. J. Birgeneau, and S. L. Holt, *ibid.* **18**, 3530 (1978).

[27]H. Grille and R. W. Gerling (unpublished).